Chapter 5

System-size dependence of collective flow parameters

The PHOBOS collaboration has performed a collective flow analysis of Cu+Cu and Au+Au interactions at $\sqrt{s_{NN}} = 200$ GeV [1]. In this chapter we also intend to perform a similar study over a wider variety of colliding systems at a typical FAIR energy ($E_{\rm lab} = 30A$ GeV) in the context of the upcoming CBM experiment. The importance of choosing this particular energy value has also been underlined in the previous chapter. We believe that it would be interesting to explore the effects of multiplicity, scattering and geometry on the collective behaviour of final state hadrons produced in small (^{28}Si+^{28}Si and ^{59}Ni+^{59}Ni), medium (^{119}In+^{119}In) and large (^{197}Au+^{197}Au) sized systems. Apart from the commonly used elliptic flow parameter, significance of non-zero odd harmonics, although not quite as large as the elliptic flow, has already been established. In order to constrain the equation of state of the fireball material, a combined analysis of the first three Fourier harmonics, namely the directed, elliptic and triangular flow is necessary [2–4]. However, in our earlier investigations we did not take the directed flow parameter (v_1) into account. It is to be noted that instead of repeating the basic ideas of second and third harmonics, we simply refer them to the previous chapters of this thesis. In the present investigation we are going to present a system-size dependence of different kinds of distributions of the first three flow harmonics, denoted respectively by v_1, v_2 and v_3. It would also be worthwhile to have a comparison between the simulated and experimental results available [1, 5–7]. Once again we have employed the AMPT model in its string melting version to simulate the symmetric AA collision events for the systems considered, where the parton scattering cross section is set to $\sigma = 3$ mb.

5.1 Results and discussions

The minimum bias event samples of our simulated data consist of 10^6 events for the ^{197}Au + ^{197}Au interaction, 2×10^6 events for the ^{115}In + ^{115}In interaction, 3×10^6 events for the ^{59}Ni + ^{59}Ni interaction and 7.5×10^6 events for the ^{28}Si + ^{28}Si interaction all at $E_{\rm lab} = 30A$ GeV. If otherwise not mentioned, we shall consider only the charged hadrons falling within the central pseudorapidity region ($|\eta - \eta_0| \leq 1.0$) for our analysis, η_0 being the centroid of the corresponding η-distribution. Figure 5.1 shows the multiplicity distributions of charged hadrons falling within the kinematic cut for the minimum bias event samples mentioned above. With increasing system size an increase in the multiplicity range is an obvious observation. The influence of initial geometric deformation and e-by-e fluctuations present

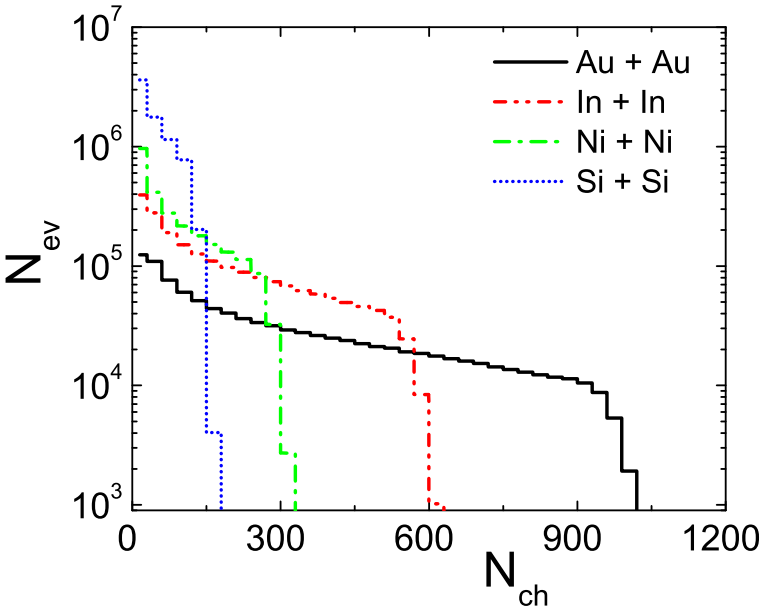

Figure 5.1: Multiplicity distribution of charged hadrons for different colliding systems at $E_{\rm lab} = 30A$ GeV.

in the initial state has been discussed in the previous chapters, but with reference to the Au+Au system only. To maintain a continuity we briefly recall the different definitions of the initial state deformations once again. The initial geometric deformation of the overlapping region of the colliding nuclei is defined in terms of the nuclear eccentricity parameter given by,

$$\varepsilon_2 = \frac{\sigma_y^2 - \sigma_x^2}{\sigma_y^2 + \sigma_x^2} \tag{5.1}$$

where σ_x and σ_y are the variances in the respective position coordinates of the nucleons present in the overlapping part [8]. Equation (5.1) defines the nuclear eccentricity ($\varepsilon_{\rm std}$), which is restricted only to $n = 2$, and intrinsically biased with an asymmetry definition that drives the flow signal. In small sized systems and peripheral collisions, due to large

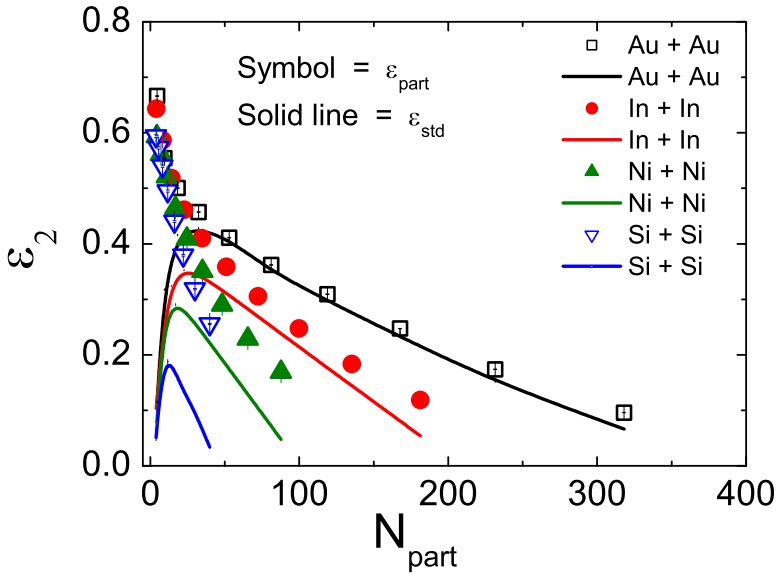

Figure 5.2: Eccentricity as a function of centrality measured in terms of $N_{\rm part}$.

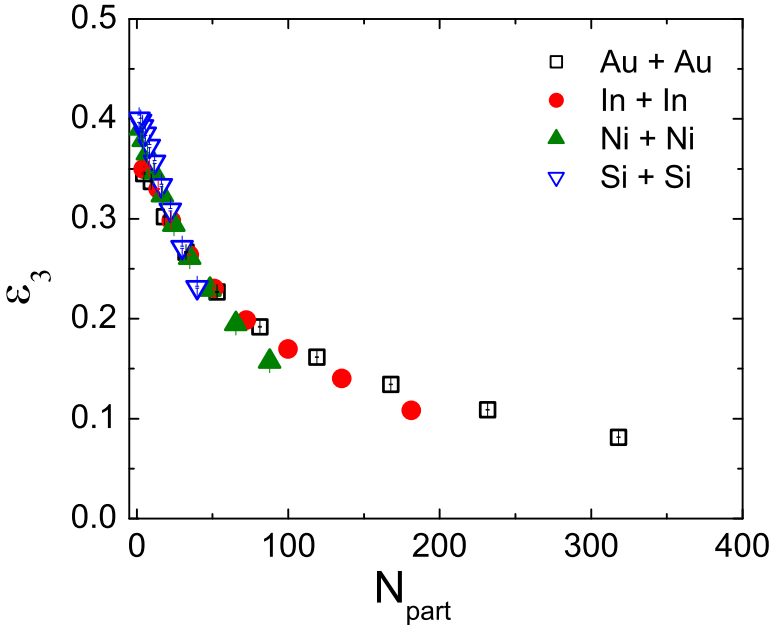

Figure 5.3: Triangularity as a function of $N_{\rm part}$.

relative fluctuations in the number and position coordinates of the participating nucleons, the minor axis of the overlapping region may not always coincide with the impact parameter. On the other hand, in the central collisions between two large nuclei the nuclear geometry and the participant geometry almost coincide with each other. A more general method of measuring the asymmetry is therefore, to consider the e-by-e initial state fluctuations in the number and position coordinates of the participating nucleons. In this scheme the geometric

anisotropy associated with the n-th harmonic is expressed as [9],

$$\varepsilon_n = \frac{\sqrt{\langle r^2 \cos(n\varphi)\rangle^2 + \langle r^2 \sin(n\varphi)\rangle^2}}{\langle r^2 \rangle} \tag{5.2}$$

Corresponding ε_2 derived from Equation (5.2), is called the participant eccentricity ($\varepsilon_{\rm part}$). In Figure 5.2 we compare the centrality dependence of both the eccentricity parameters, namely $\varepsilon_{\rm std}$ and $\varepsilon_{\rm part}$. The $N_{\rm part}$-dependence of the eccentricity parameters can be attributed to geometrical reasons. For all four colliding systems considered in the present analysis, we see that the participant eccentricities are quite high valued in the most peripheral collisions ($\varepsilon_{\rm part} \approx 60 - 70\%$). As expected, with increasing $N_{\rm part}$ the participant eccentricities monotonically drop down to rather small values ($\varepsilon_{\rm part} \approx 10 - 20\%$) in each case. For a smaller colliding system the rate of fall is steeper. Peripheral collisions always involve smaller $N_{\rm part}$. Therefore, for a single event the periodic functions of Equation 5.2 can be averaged over a smaller number of terms. Accordingly the chance that every event will contribute significantly to $\varepsilon_{\rm part}$, is higher. With increasing centrality $N_{\rm part}$ increases, and for every event the periodic functions are averaged over an increasing number of terms. As a result, the contribution to $\varepsilon_{\rm part}$ from every event becomes smaller. On the other hand, in the most peripheral collisions nuclear eccentricities are quite small valued ($\varepsilon_{\rm std} \lesssim 10\%$). In a small overlapping volume the transverse coordinates of the participating nucleons, irrespective of its geometrical asymmetry, are distributed within narrow regions in every direction. Corresponding variances should therefore, be very close to each other and their differences are even smaller. With increasing centrality $\varepsilon_{\rm std}$ rises rapidly, attains a maximum, and then falls off gradually at large $N_{\rm part}$ for each colliding system. The distributions are right skewed, and the skewness is higher for a larger system. We notice that only for the largest system (Au+Au), the eccentricity values defined in two different ways agree with each other, that too beyond a certain centrality measure ($N_{\rm part} \gtrsim 60$). In all other cases $\varepsilon_{\rm std}$ is consistently smaller than $\varepsilon_{\rm part}$. As the initial fluctuations are seen to play an important role, one should be careful in choosing the correct eccentricity expression. It has been argued that if the flow is independent of particle species, $\varepsilon_{\rm part}$ and not $\varepsilon_{\rm std}$, is a more appropriate parameter that can explain the behaviour of elliptic flow [1]. The geometric deformation associated with the third harmonic ($n = 3$), also called the triangularity parameter (ε_3), can be obtained from Equation (5.2). In Figure 5.3 the ε_3 values are plotted as a function of $N_{\rm part}$ for all the colliding systems. We observe that the variation of ε_3 with $N_{\rm part}$ is nearly independent of the system size. Starting from a moderately high value $\varepsilon_3 \approx (35 - 40)\%$, the triangularity parameter decreases monotonically with increasing $N_{\rm part}$. Though the $N_{\rm part}$ dependence of ε_3 is quite similar to that of $\varepsilon_{\rm part}$, as expected $\varepsilon_{\rm part}$ is almost always higher in magnitude than ε_3. Our observation on ε_2 and ε_3 agrees reasonably well with another simulation study

Table 5.1: $N_{\rm part}$ dependence of the asymmetry parameters and midrapidity particle densities in different colliding systems at $E_{\rm lab} = 30A$ GeV.

Centrality	$N_{\rm part}$	$\varepsilon_{\rm std}$	$\varepsilon_{\rm part}$	ε_3	$\frac{dN_{\rm ch}}{d\eta}\|_{\eta_0}$
			Au+Au		
0-10%	318.0±0.08	0.066±0.0003	0.096±0.0002	0.081±0.0001	238.4±0.09
10-20%	231.6±0.07	0.176±0.0003	0.174±0.0002	0.109±0.0002	171.5±0.07
20-30%	167.7±0.06	0.257±0.0004	0.247±0.0003	0.134±0.0002	126.8±0.06
30-40%	118.9±0.05	0.322±0.0005	0.309±0.0004	0.162±0.0003	92.3±0.05
40-50%	81.2±0.04	0.371±0.0006	0.362±0.0004	0.192±0.0003	65.4±0.04
50-60%	52.9±0.04	0.408±0.0007	0.411±0.0005	0.227±0.0004	44.4±0.04
60-70%	32.4±0.03	0.428±0.0009	0.457±0.0005	0.267±0.0004	28.5±0.03
70-80%	18.3±0.02	0.416±0.0013	0.501±0.0007	0.302±0.0006	18.5±0.03
80-90%	9.5±0.02	0.318±0.0014	0.554±0.0006	0.339±0.0005	10.7±0.02
90-100%	4.5±0.01	0.115±0.0021	0.666±0.0008	0.369±0.0007	5.4±0.01
			In+In		
0-10%	181.2±0.04	0.054±0.0002	0.119±0.0001	0.108±0.0001	145.5±0.04
10-20%	135.3±0.04	0.144±0.0003	0.183±0.0002	0.14±0.0002	109.0±0.04
20-30%	99.8±0.03	0.214±0.0004	0.248±0.0003	0.17±0.0002	82.1±0.03
30-40%	72.3±0.03	0.269±0.0004	0.306±0.0003	0.199±0.0002	61.3±0.03
40-50%	51.0±0.03	0.311±0.0005	0.359±0.0003	0.23±0.0003	44.9±0.03
50-60%	34.7±0.02	0.341±0.0006	0.41±0.0004	0.264±0.0003	31.9±0.02
60-70%	22.7±0.02	0.353±0.0008	0.461±0.0004	0.298±0.0003	21.8±0.02
70-80%	14.1±0.02	0.324±0.001	0.518±0.0005	0.33±0.0004	14.3±0.02
80-90%	8.3±0.01	0.227±0.0012	0.587±0.0005	0.351±0.0004	9.0±0.01
90-100%	4.1±0.01	0.103±0.0013	0.634±0.0006	0.35±0.0005	5.3±0.01
			Ni+Ni		
0-10%	87.7±0.04	0.048±0.0007	0.169±0.0004	0.157±0.0004	73.4±0.02
10-20%	65.5±0.04	0.129±0.0008	0.229±0.0005	0.195±0.0005	55.2±0.02
20-30%	48.3±0.04	0.191±0.001	0.29±0.0006	0.229±0.0005	41.6±0.02
30-40%	35.0±0.04	0.239±0.0012	0.351±0.0007	0.261±0.0006	31.0±0.02
40-50%	24.6±0.04	0.275±0.0014	0.409±0.0008	0.294±0.0007	22.5±0.02
50-60%	16.9±0.03	0.29±0.0018	0.465±0.0009	0.324±0.0007	16.1±0.01
60-70%	11.2±0.03	0.263±0.0021	0.521±0.001	0.347±0.0008	11.1±0.01
70-80%	7.1±0.02	0.185±0.0026	0.561±0.0011	0.366±0.0009	7.7±0.01
80-90%	4.4±0.02	0.078±0.0031	0.594±0.0013	0.379±0.0011	5.4±0.01
90-100%	2.5±0.02	0.016±0.0036	0.604±0.0016	0.391±0.0015	4.0±0.01
			Si+Si		
0-10%	39.9±0.04	0.034±0.0018	0.256±0.001	0.232±0.0009	33.6±0.01
10-20%	29.9±0.05	0.097±0.0022	0.318±0.0013	0.272±0.0011	25.5±0.01
20-30%	22.2±0.05	0.135±0.0026	0.379±0.0014	0.309±0.0012	19.2±0.01
30-40%	16.3±0.05	0.173±0.0031	0.44±0.0016	0.333±0.0013	14.4±0.01
40-50%	11.7±0.04	0.188±0.0037	0.495±0.0017	0.357±0.0014	10.6±0.01
50-60%	8.3±0.04	0.157±0.0043	0.54±0.0019	0.373±0.0016	7.9±0.01
60-70%	5.7±0.03	0.104±0.005	0.573±0.0021	0.385±0.0018	5.9±0.01
70-80%	3.8±0.03	0.051±0.0059	0.594±0.0025	0.393±0.0022	4.6±0.01
80-90%	2.5±0.03	0.016±0.0069	0.604±0.0031	0.398±0.0028	3.7±0.01
90-100%	1.5±0.03	0.008±0.0081	0.613±0.0041	0.4±0.0037	3.1±0.01

made at the RHIC energies [10]. The $N_{\rm part}$-dependence of the geometrical asymmetry parameters associated with the overlapping regions, obtained from the MCG model [11] are listed in Table 5.1. Corresponding percentage centralities and the charged particle densities in the central particle producing region are also incorporated in this table.

5.1.1 Distributions of the flow parameters

The directed flow parameter (v_1) measures the total amount of in-plane transverse flow. As the participating nucleons try to stop each other, due to a bounce-off effect exerted by the compressed and heated fireball, the spectator nucleons of the impinging nuclei are deflected away from the beam axis. In contrast to the bounce-off effect, v_1 is not just the averaged projection of particle momentum on the impact parameter axis, considered to be the x-axis. It is rather an averaged ratio ($v_1 = \langle p_x/p_T \rangle$) of the same projection taken with respect to the transverse momentum of the particles concerned. Apart from a difference in their magnitude, the basic features of bounce-off effect and directed flow are similar [12]. The directed flow of high-p_T particles produced at the very early stages, continues to evolve until the very late stages of an AB collision. Therefore, the directed flow can be used to look into the early time thermalization or even into the pre-equilibrium stage. In non-central collisions the directed flow is most pronounced around the target and projectile rapidities.

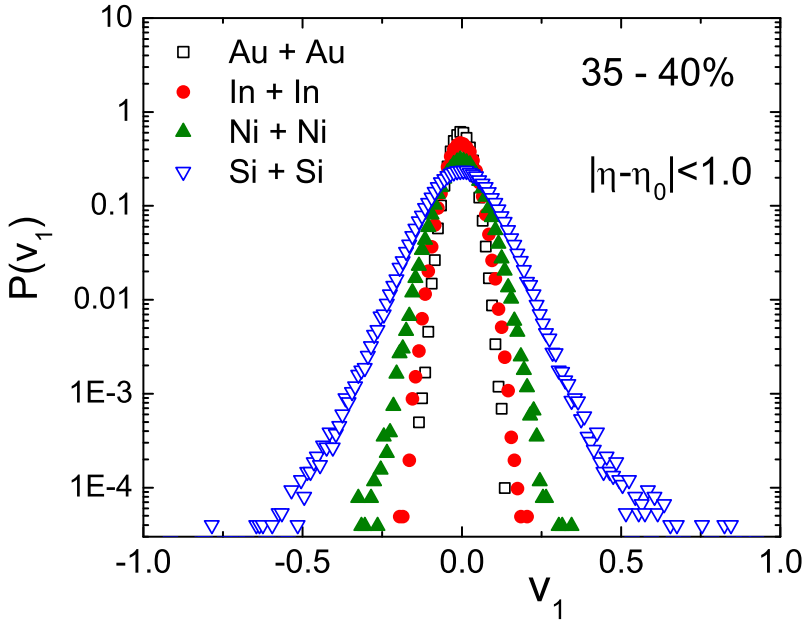

Figure 5.4: Distributions of v_1 of charged hadrons in the final state.

In Figure 5.4 we plot the probability distributions $P(v_1)$ of the directed flow parameter for the events falling within the $(35-40)\%$ centrality class for all the colliding systems. The

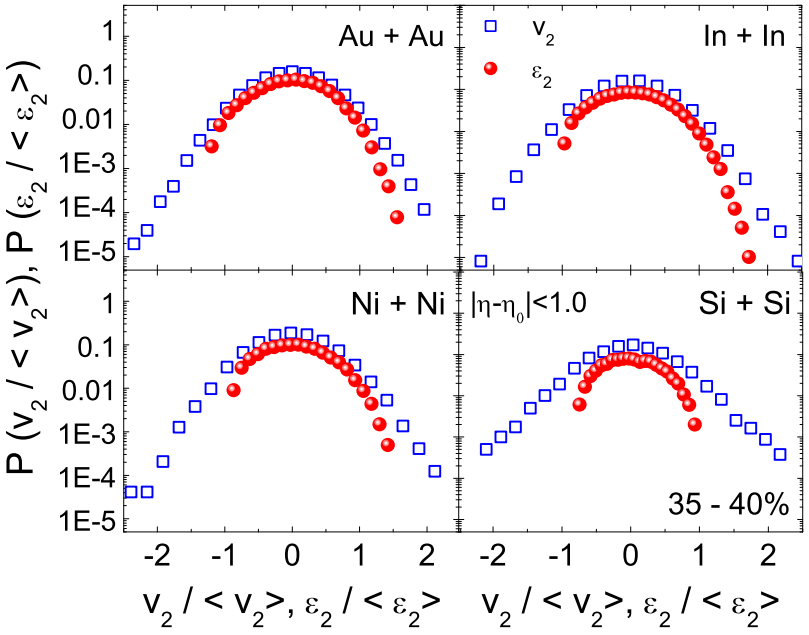

Figure 5.5: (Color online) Distributions of $v_2/\langle v_2\rangle$ and $\varepsilon_2/\langle\varepsilon_2\rangle$ of final state charged hadrons.

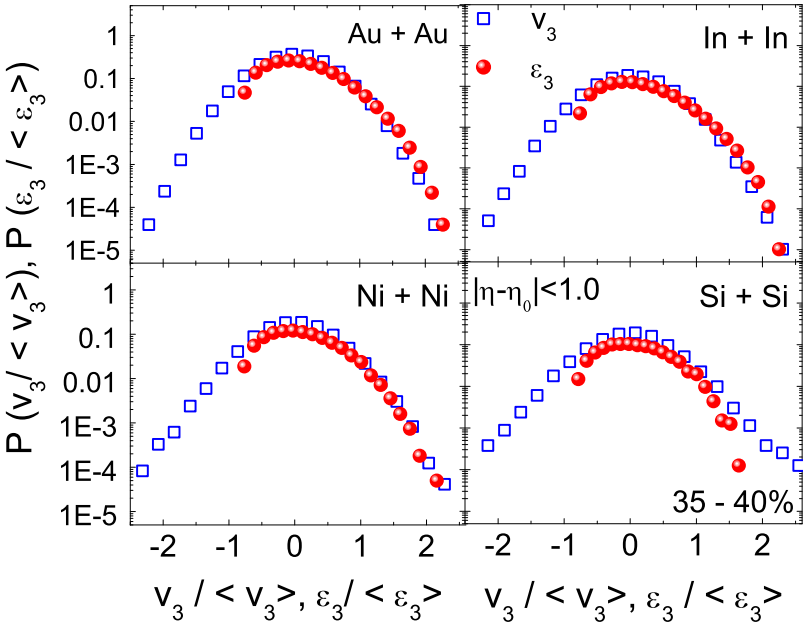

Figure 5.6: Distributions of $v_3/\langle v_3\rangle$ and $\varepsilon_3/\langle\varepsilon_3\rangle$ of final state charged hadrons.

distributions look like sharply peaked Gaussian functions, symmetrically centered around $v_1 = 0$. The width of the distributions however moderately increases with decreasing system size, an observation that may be attributed to statistical reasons. In a larger system, within a particular centrality class, on an average a larger number of participating nucleons will be involved, producing thereby a larger number of hadrons. As a result, in a larger system the averaging in v_1 is performed over a larger number of particles, which results in smaller

v_1-values and correspondingly smaller fluctuations. Corresponding distributions of other flow parameters $P(v_2)$ and $P(v_3)$, are presented respectively in Figure 5.5 and Figure 5.6 in the $(35-40)\%$ centrality interval for all the colliding systems considered in the present investigation. We now compare these distributions with the distributions of corresponding asymmetry parameters [13]. Both v_n and ε_n for $n = 2$ and 3 are normalized by their respective mean values. The normalized flow parameters $v_2/\langle v_2\rangle$ and $v_3/\langle v_3\rangle$ are almost symmetrically distributed around their respective zeroes, but they are not as sharply peaked as the v_1-distributions. The distributions of the normalized asymmetry parameters, namely $\varepsilon_2/\langle\varepsilon_2\rangle$ and $\varepsilon_3/\langle\varepsilon_3\rangle$, are slightly right skewed. Hydrodynamics predicts that for an ideal fluid at a given energy v_2 should scale with ε_2 [8, 14]. A strict proportionality like $v_n \propto \varepsilon_n$ should result in a complete overlapping between $P(v_n/\langle v_n\rangle)$ and $P(\varepsilon_n/\langle\varepsilon_n\rangle)$. Such an exact overlapping however is not observed in any of our colliding systems. Limited overlapping is found in all the colliding systems for both $n = 2$ and 3, which gradually weakens as the system size becomes smaller. We may therefore conclude that, as expected the fireball material created at $E_{\rm lab} = 30A$ GeV in the framework of AMPT, does not exactly behave like an ideal fluid.

5.1.2 The directed flow

In this section we present our simulation results on $N_{\rm part}$, η and p_T-dependence of v_1 for the charged hadrons produced in all four colliding systems under consideration. We have calculated the p_T-integrated v_1-values in the mid-pseudorapidity region ($|\eta - \eta_0| \leq 1.0$). In Figure 5.7 we plot the v_1-values so obtained against $N_{\rm part}$. We notice that except for a few highest centrality classes, however small it may be, v_1 is consistently negative valued. In medium and large systems like In+In and Au+Au, there is an initial uniformity in the v_1 against $N_{\rm part}$ plot, which subsequently is followed by an almost linear rise towards $v_1 \approx 0$. On the other hand, v_1 steadily approaches zero in smaller systems like Si+Si and Ni+Ni. In symmetric nuclear collisions, in the $E_{\rm lab} = 30A$ GeV range, due to the nuclear shadowing effect an antiflow develops in the pion dominated systems as it is in the present case [15], and we get negative values of v_1 [16]. As we move from the most peripheral to the most central class of events, due to multiple rescattering the nuclear shadowing (screening) gradually disappears, and the flow effect starts to counterbalance the antiflow. As a result we see a monotonic, almost linear fall in the magnitude of v_1. We notice that at a particular $N_{\rm part}$, in a larger colliding system v_1 is larger in magnitude. Hadrons with small rapidities, produced early in the direction of normal flow, will be absorbed by the spectator nuclei. However, this process is less efficient in heavier systems. Therefore, the directed flow displays a softening in smaller sized colliding objects [12]. Our simulation results on directed flow represent a violation of the entropy-driven multiplicity scaling for different

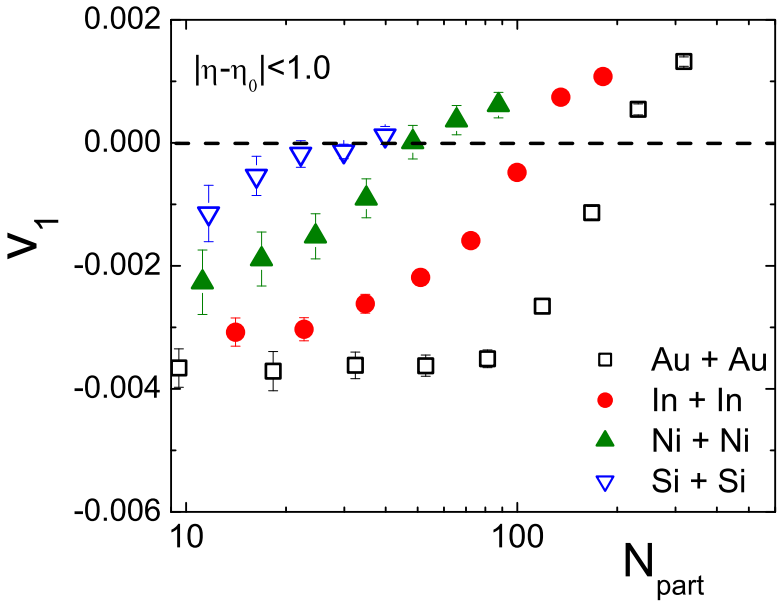

Figure 5.7: $N_{\rm part}$ dependence of v_1 of charged hadrons for different colliding systems.

colliding systems. The PHOBOS data showed that at all centralities, v_1 is independent of the system size [17], although a transport model simulation did not exactly substantiate such a system-size independence.

Figure 5.8 depicts the η-dependence of v_1 at different centrality intervals, i.e. in extreme

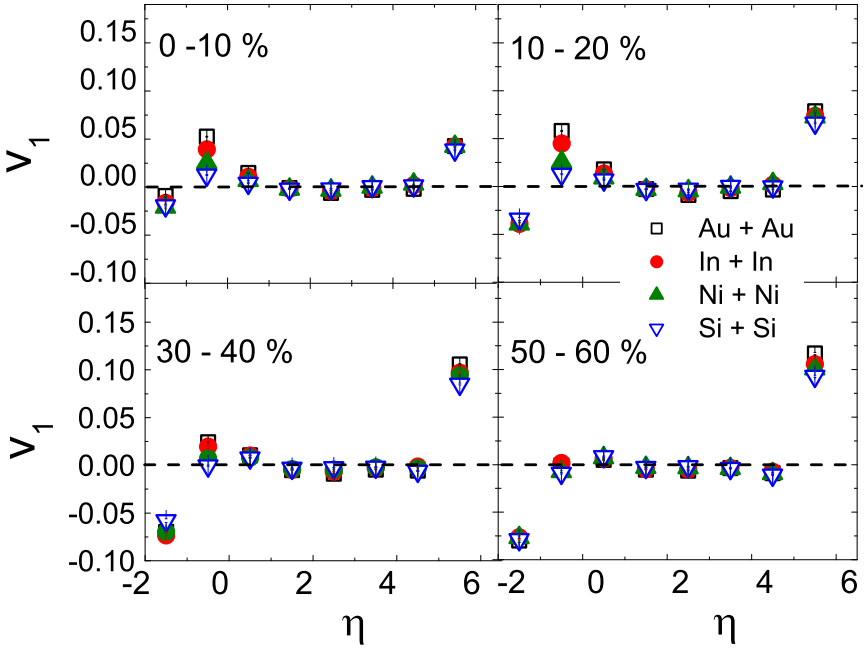

Figure 5.8: η dependence of v_1 of charged hadrons for different colliding systems.

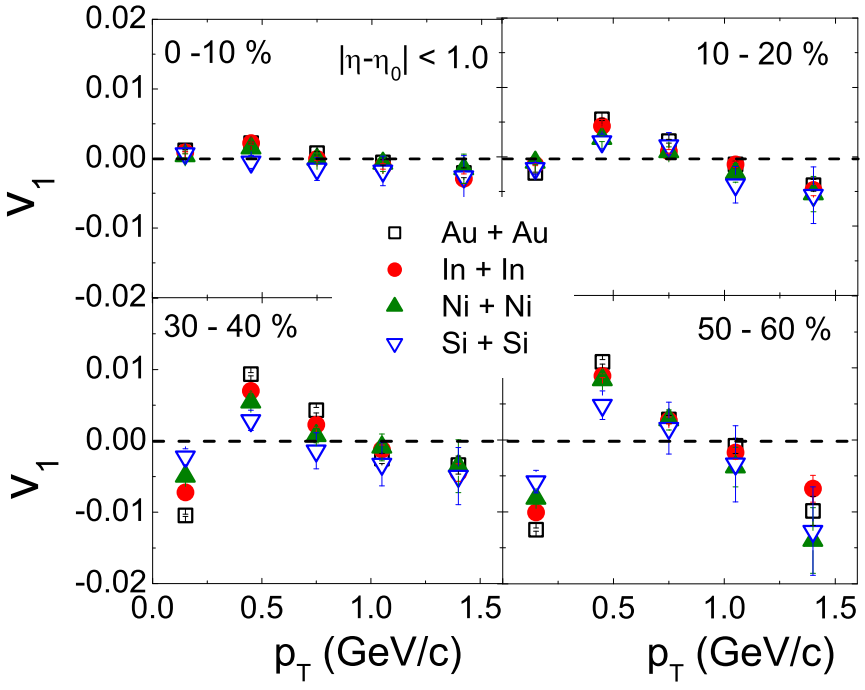

Figure 5.9: p_T dependence of v_1 of charged hadrons for different colliding systems.

central, mid-central and peripheral AA collisions. At $E_{\rm lab} = 30A$ GeV in the mid-η region v_1 is very small valued and its variation with η appears to wiggle around the $v_1 = 0$ line. The slope of the v_1 vs. η curve is negative in the mid-η region, and positive in the fragmentation regions. However, the variation of v_1 with η is not exactly linear in the mid-η region. With increasing centrality the slope of the curve in the mid-η region increases in magnitude, and gradually a system size dependence becomes prominent. For a larger system the slope becomes larger. On the other hand in the peripheral collisions the v_1 vs. η variation becomes almost independent of the system size. In high-energy AB collisions more hadrons are produced and the spectator parts of the nuclei quickly leave the interaction zone, though in opposite directions, thus giving space to the flow to develop in both directions. Directed flow at the midrapidity drops almost to zero. In the hydrodynamical approach the wiggle is explained by using a QGP equation of state [18, 19]. On the other hand, in the cascade models the wiggle is explained in terms of a space-momentum correlation coupled with different amount of rapidity loss of the incoming nucleons in different space regions [20]. Our simulation based observations on the η-dependence of v_1, are found to be in unison with the existing RHIC [21] and LHC [22] results. Yet the magnitude of $v_1(\eta)$ is systematically higher in our case, a characteristic feature of v_1 as reported over a wide range of energies[21–26].

In Figure 5.9, we present the p_T-dependence of v_1 within $|\eta - \eta_0| < 1.0$ at four different centralities and for all the collision systems considered in this analysis. In the extreme central $(0-10\%)$ and central $(10-20\%)$ collisions we do not see any definite p_T-dependence

of v_1, except that its value fluctuates around the $v_1 = 0$ line. However, in mid-central $(30 - 40\%)$ and peripheral $(50 - 60\%)$ collisions, as p_T increases there is a sign change in the v_1-values. Within $0.2 < p_{_T} < 0.5$ GeV/c, v_1 increases with p_T from negative to positive values, and then it decreases with increasing p_T, once again crossing the $v_1 = 0$ line at $p_T \gtrsim 1.0$ GeV/c. It has been pointed out that for soft production ($0 \leq p_T \leq 1.5$ GeV/c), the probable reason of v_1 crossing the zero line a couple of times could be an artifact of combining all charged hadrons in our analysis, whereas v_1 of pions and baryons bear different signs [23, 24]. Another feature of our $v_1(p_{_T})$ result is that there is a definite system size dependence in the mid-central and peripheral collisions, which is not very prominent in the central collisions. A study of directed flow of identified particles for different species of particles may provide a better insight to these observations.

5.1.3 Centrality dependence of v_2 and v_3

We first compute the v_2-parameter as a function of $N_{\rm part}$ in the central region ($|\eta - \eta_0| \leq 1$) for all the colliding systems considered in this analysis. The results are shown in Figure 5.10(a). Smaller v_2-values are observed in extreme central and peripheral collisions. They are maximum in the semi-central collisions. Our observations are similar to the RHIC [17] and LHC [27] experiments. They can be explained in terms of the geometric effects and the pressure gradients developed thereof [28]. It is noticed that with increasing system-size the peak of the v_2 distribution shifts towards higher centrality. This kind of observation has been attributed to a hydro-dynamical evolution of the system [29, 30]. At a particular $N_{\rm part}$, the magnitude of v_2 is found to be higher in a larger system, an observation which again is similar to that of a RHIC experiment [17]. However, in comparison with the RHIC results, the magnitude of our AMPT simulated v_2 at an expected FAIR energy, is lower by a factor of 2. Experimental results obtained from the Alternating Gradient Synchrotron (AGS) to the LHC energies, have established that the centrality dependence of v_2 provides valuable information regarding the degree of thermalization achieved in AB systems. It is understood that such equilibration is possible due to multiple rescattering among the constituent particles present in the system. Hydrodynamics predicts that v_2/ε_2 should saturate when the collision system achieves a local equilibrium. If the produced matter equilibrates, it should behave almost like an ideal fluid [8, 14]. In order to better understand how rescattering influences the results on flow parameters, it is therefore necessary to scale out the effects of geometry from our calculations [31]. In Figure 5.10(b) we plot the $v_2/\varepsilon_{\rm std}$-ratio against $N_{\rm part}$. It is noticed that the bell shaped pattern of v_2 vs. $N_{\rm part}$ plot, as observed in Figure 5.10(a), disappears. Instead, the $v_2/\varepsilon_{\rm std}$-ratio increases monotonically with increasing $N_{\rm part}$. The variation of $v_2/\varepsilon_{\rm std}$ is non-lnear, and in smaller systems the ratio rises quite rapidly with $N_{\rm part}$. As the system-size increases the variation becomes flat, and for

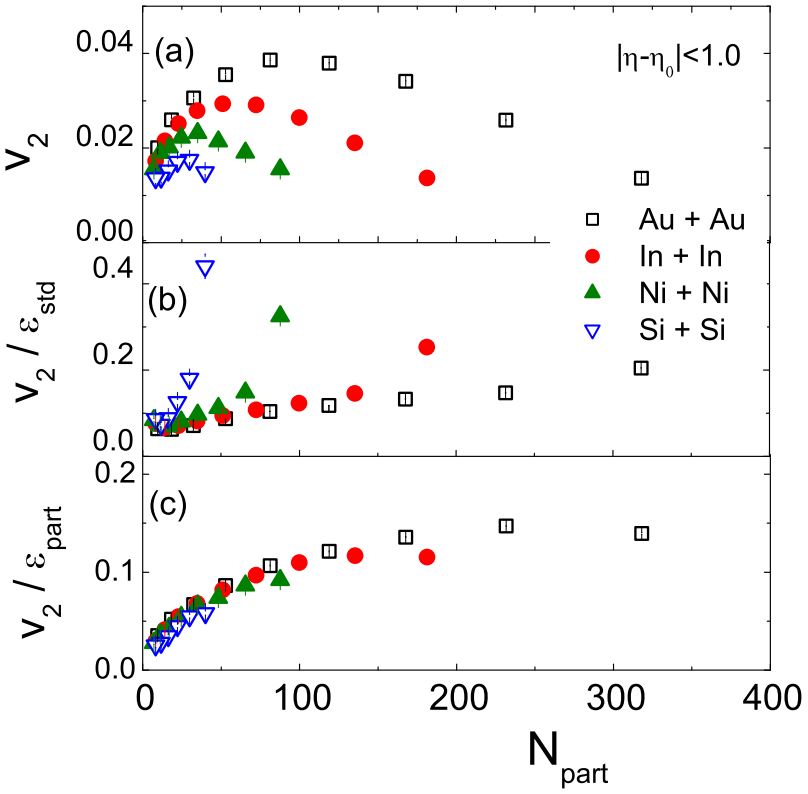

Figure 5.10: $N_{\rm part}$ dependence of (a) the elliptic flow parameter v_2, (b) v_2 scaled by the standard eccentricity $\varepsilon_{\rm std}$, and (c) v_2 scaled by the participant eccentricity $\varepsilon_{\rm part}$, for charged hadrons in various AB collisions at $E_{\rm lab} = 30A$ GeV.

the Au+Au and In+In systems it is almost linear. However, the expected saturation is not observed, which we have previously ascribed to an eccentricity expression that does not take care of the fluctuations of the participating nucleons [1]. As soon as we replace $\varepsilon_{\rm std}$ by $\varepsilon_{\rm part}$, a near scaling (system-size independence) of $v_2/\varepsilon_{\rm part}$ is noticed in Figure 5.10(c). Once the nuclear geometry is taken care of, we are left only with the multiplicity dependence, a feature also known as the multiplicity scaling [32]. The scaling nature makes it easier for us to realise that at a particular collision energy the rescattering mechanism remains unaltered in different colliding systems. Furthermore, once again it is established that $\varepsilon_{\rm part}$ is the appropriate eccentricity parameter to be used. Unless otherwise specified, for the rest of our discussion we shall use $\varepsilon_{\rm part}$ as the eccentricity measure and denote the same by ε_n : $n = 2, 3$.

In Figure 5.11 we plot the v_2/ε_2-ratio against S^{-1} $(dN_{\rm ch}/dy)$, the produced particle density per unit transverse area of the nuclear overlapping region. The initial overlapping area of the colliding nuclei S is calculated by using the MCG model [11]. Results obtained from all the colliding systems considered in this analysis are plotted together with those obtained from other experiments [24, 33–35]. The idea is to compare data obtained from different collision

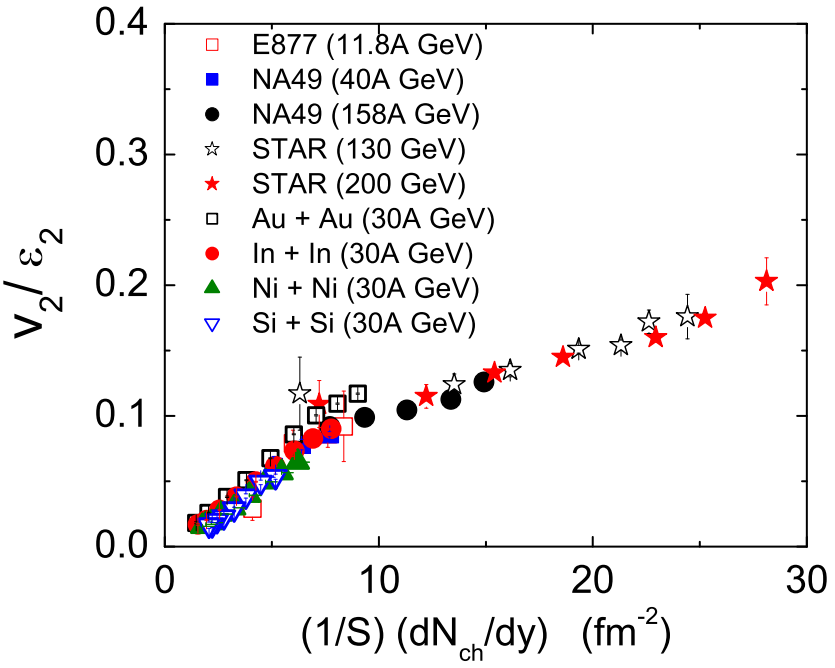

Figure 5.11: Variation of eccentricity scaled elliptic flow with transverse particle density.

systems at different energies and at different centralities. Whereas v_2 reflects the space-momentum correlation developed due to the early stage pressure gradient, S^{-1} $(dN_{\rm ch}/dy)$ is a measure of the transverse particle density. Hence v_2/ε_2 versus S^{-1} $(dN_{\rm ch}/dy)$ plot should be seen as an alternative to the pressure versus energy density plot. In other words it is sensitive to the sound velocity in the medium as well as the equation of state of the matter produced during the expansion stage. A non-smooth behaviour of the plot would indicate a change in the medium properties. In this connection we recall that the energy density achieved in AB collisions is determined by the Bjorken's formula [36], which looks very similar to the transverse particle density S^{-1} $(dN_{\rm ch}/dy)$. We see that for the entire range of data a linear dependence like

$$\frac{v_2}{\varepsilon_2} \propto \frac{1}{S}\frac{dN_{ch}}{dy} \tag{5.3}$$

is only approximately obeyed and not exact. The proportionality constant should depend on the the region of fit, the hydro-limit of v_2/ε_2 ratio, the partonic scattering cross-section and the velocity of elastic wave in the medium [37]. The key feature of the plot is that, except for a few highest centrality classes in Au + Au collision, our results nearly agree with the results available from the E877 and NA49 experiments. Similar observation is made in [28], where in addition to the AMPT (string melting) version the UrQMD and the AMPT default version are used.

We now examine the centrality dependence of v_3. In Figure 5.3 it has been shown that the initial spatial anisotropy ε_3 is higher in peripheral collisions, and almost independent

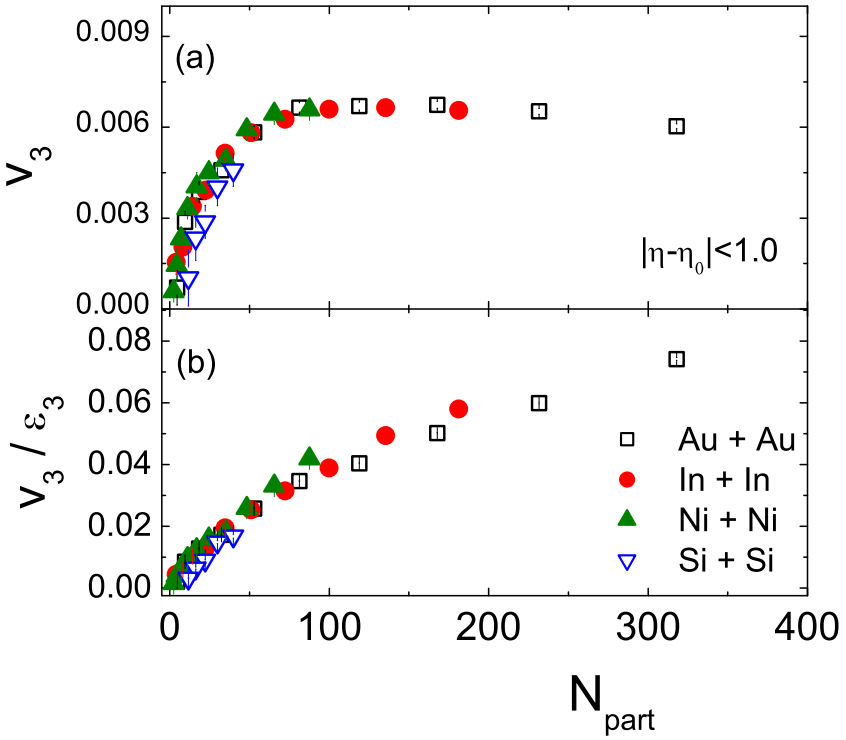

Figure 5.12: (a) Triangular flow and (b) triangular flow scaled by triangularity of charged hadrons against $N_{\rm part}$ for various AB collisions at $E_{\rm lab} = 30A$ GeV.

of the system size. A similar feature can be seen in Figure 5.12(a) too, where v_3 is plotted against $N_{\rm part}$. We notice that the $N_{\rm part}$-dependence of v_3 is also almost independent of the system size. v_3 is small in peripheral collisions, rises with $N_{\rm part}$, and saturates at higher centralities. The conversion from initial space asymmetry to final state momentum anisotropy is less efficient in peripheral collisions. However, the same appears to be equally inefficient in all the collision systems considered in our analysis. We also notice that for a particular collision system, v_2 is consistently larger in magnitude than v_3. This is understood from the fact that v_2 arises from the geometrical asymmetry as well as from the initial state fluctuations, while v_3 originates only from the initial state fluctuations. A more detailed representation of this issue is seen in the relative magnitude of v_3 and v_2 plotted as a function of $N_{\rm part}$ in Figure 5.13. In all cases initially the relative strength of v_3 increases slowly with centrality, and the rate of increase suddenly rises towards more central events, almost like a power-law. Gross features of our observation in this regard are compatible to the simulation results at RHIC energies [9], and once again can be ascribed to the multiplicity scaling. In Figure 5.12(b) an nearly linear rise in the v_3/ε_3-ratio with increasing $N_{\rm part}$ is observed, which again is almost independent of the system size. In Figure 5.12 the saturation that we see in the centrality dependence of the triangular flow parameter, can therefore be attributed to the geometrical effects, and our results in this regard also appear to be consistent with the multiplicity scaling [32].

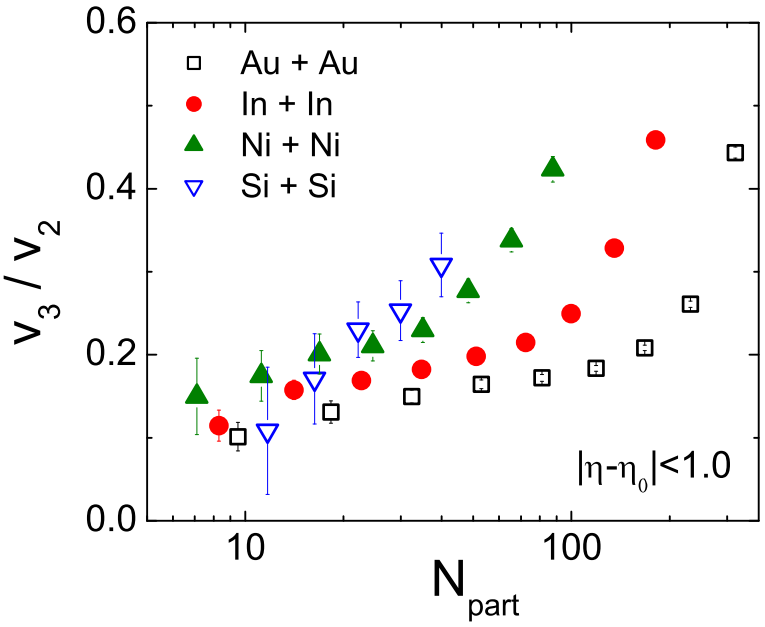

Figure 5.13: Ratio of v_3 to v_2 of charged hadrons as a function of $N_{\rm part}$ for different colliding systems at $E_{\rm lab} = 30A$ GeV.

5.1.4 Transverse momentum dependence of v_2 and v_3

The p_T-dependence of flow parameters plays a vital role to understand the influence of transverse degrees of freedom on the collective motion of final state particles. Simulation based results at FAIR conditions reported so far can be found in [28, 38, 39]. Whereas resonance decays are expected to dominate the low-p_T behaviour, at high-p_T particles originate from fragmentation of jets modified in the hot and dense fireball medium [40]. Another important feature of the p_T-dependence of flow parameters, is the mass ordering of baryons in the low p_T sector, i.e. upto $p_T \gtrsim 1.0$ GeV/c at $E_{\rm lab} = 30A$ GeV. Beyond this range, the mass ordering is found to be broken. Actually the ordering gets inverted as $p_T > 1.4$ GeV/c – the p_T dependence of baryons and mesons are found to split into two separate bands [38]. Hydrodynamical model(s) can describe the related issues at RHIC energies [41, 42] In this investigation we would like to study the effects of (re)scattering or equivalently that of the multiplicity on the p_T-dependence of v_2 and v_3. It would have been ideal, if for each colliding system under investigation, we could fix a precise $N_{\rm part}$ for all the variables studied in this work. However, as the maximum $N_{\rm part}$ is widely distributed in our chosen collision systems, starting from 56 in Si + Si and ending up at 394 in Au + Au, for a proper justification we have categorized our data into different $N_{\rm part}$-groups. To study the p_T-dependence we have chosen $\langle N_{\rm part}\rangle = 100$ for the Au+Au and In+In, and $\langle N_{\rm part}\rangle = 35$ for the Ni+Ni and Si+Si systems. Both choices correspond to semi-central collisions, where high values of flow parameters are expected. In the upper panels of Figure 5.14 and Figure 5.15 we schematically present the p_T-dependence of v_2 and v_3, and in the lower panels of the same figures

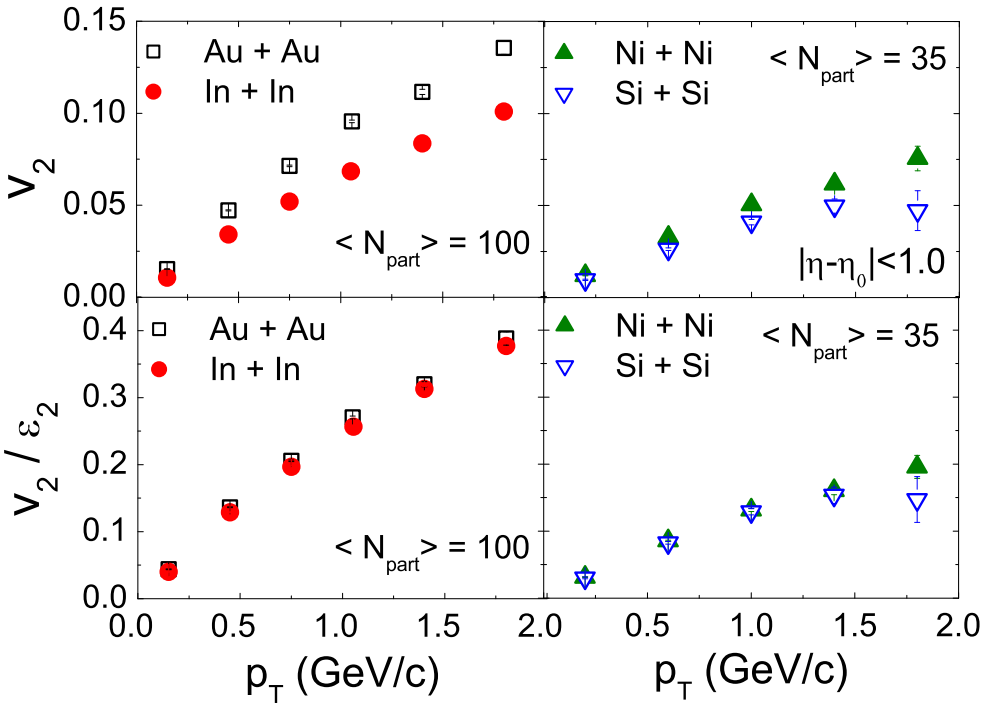

Figure 5.14: p_T dependence of v_2 (upper panel) and v_2/ε_2 (lower panel) of charged hadrons for different colliding systems at $E_{\rm lab} = 30A$ GeV.

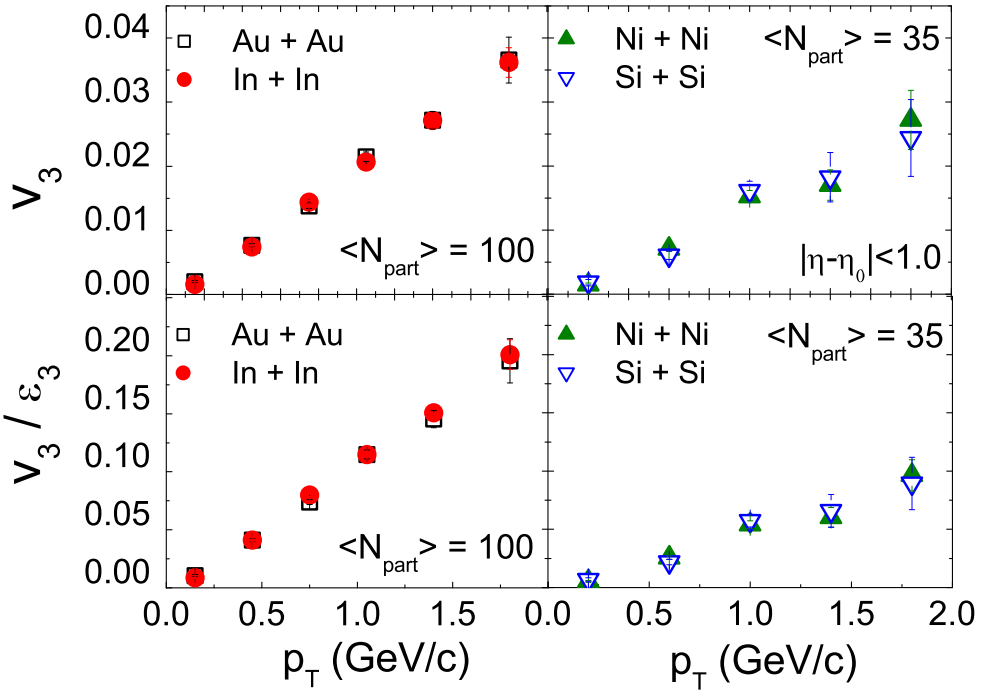

Figure 5.15: p_T dependence of v_3 (upper panel) and v_3/ε_3 (lower panel) of charged hadrons for different colliding systems at $E_{\rm lab} = 30A$ GeV.

similar plots for the ratio $v_n/\varepsilon_n\,(n = 2, 3)$ are made. The p_T-dependence of v_2 shows its usual nature, increasing almost linearly with $p_{_T}$. The rate of increase is higher in a larger system. However, once again as the geometric effects are removed, the v_2/ε_2-ratio becomes independent of the system size, an observation also reported by the PHOBOS collaboration in Au+Au and Cu+Cu systems at $\sqrt{s} = 200$ GeV [1]. This scaling nature can be attributed to a common particle production mechanism and the collective flow developed thereof. At a particular $\langle N_{\rm part}\rangle$ the transverse particle density is expected to be approximately same. The v_2/ε_2-ratio being linearly dependent on it, should have the identical values. It is believed that the in-medium viscous effects present in large magnitude should introduce a system-size dependence on $v_2(p_{_T})$ [43–45]. Furthermore, the viscosity will cause v_2 to saturate at low-$p_{_T}$ in small sized systems. A system-size independent scaling of $v_2(p_{_T})$ is therefore, a manifestation of insignificant presence (or absence) of viscous effects in the hadronic/partonic medium created in the AB interactions of our consideration after the collective flow is developed. The pattern of $p_{_T}$-dependence of v_3 is almost similar to that of v_2. However, we observe that neither v_3 nor v_3/ε_3-ratio has any significant dependence on the system size.

5.2 Conclusion

In this investigation we have presented some simulation results on the system-size dependence of some gross aspects of the first three harmonic flow parameters in ^{28}Si+^{28}Si, ^{59}Ni+^{59}Ni, ^{115}In+^{115}In and ^{197}Au+^{197}Au interactions at $E_{\rm lab} = 30A$ GeV. The AMPT model in its string melting version has been used to generate the event samples. Our results however, do not warrant any significant change in the properties of the fireball medium, even though the collision size is changed significantly. It has been pointed out that many aspects of soft-hadron production (within $0 \leq p_T \leq 2.0$ GeV/c) depend only on the rapidity density [32]. There should be no significant dependence on the beam energy, centrality, or mass of the colliding nuclei. This type of scaling is known as entropy-driven soft physics. Except for the centrality dependence of the directed flow parameters, almost all of our flow results are found either due to the geometrical effects, or they are an outcome of the multiplicity scaling, or both. The present analysis pertains to all charged hadrons, and no segregation in terms of different particle species has been made. It is expected that the flow behaviours of hadrons with different intrinsic properties should also be different.

Bibliography

[1] B. Alver *et al.* (PHOBOS Collaboration), Phys. Rev. Lett. **98**, 242302 (2007).

[2] B. Schenke, S. Jeon, and C. Gale, Phys. Rev. Lett. **106**, 042301 (2011).

[3] B. Schenke, S. Jeon, and C. Gale, Phys. Rev. C **82**, 014903 (2010); **85**, 024901 (2012).

[4] B. Alver *et al.*, Phys. Rev. C **82**, 034913 (2010).

[5] L.-W. Chen and C. M. Ko, Phys. Lett. B **634**, 205 (2006).

[6] A. Adare *et al.* (PHENIX Collaboration), Phys. Rev. Lett. **98**, 162301 (2007).

[7] A. Adare *et al.* (PHENIX Collaboration), Phys. Rev. C **94**, 054910 (2016).

[8] H. Sorge, Phys. Rev. Lett. **82**, 2048 (1999).

[9] B. Alver and G. Roland, Phys. Rev. C **81**, 054905 (2010).

[10] L. X. Han *et al.*, Phys. Rev. C **84**, 064907 (2011).

[11] A. Shor and R. Longacre, Phys. Lett. B **218**, 100 (1989); C. Loizides, Phys. Rev. C **94**, 024914 (2016) .

[12] L. V. Bravina and E. E. Zabordin, Eur. Phys. J. A **52**(8), 245 (2016).

[13] C. Gale *et al.*, Phys. Rev. Lett. **110**, 012302 (2013).

[14] J.-Y. Ollitrault, Phys. Rev. D **46**, 229 (1992).

[15] S Ghosh *et al.*, J. Phys. G: Nucl. Part. Phys. **48**, 125106 (2021).

[16] J. Y. Ollitrault, Nucl. Phys. A **638**, 195 (1998).

[17] B. I. Abelev *et al.* (STAR Collaboration), Phys. Rev. C **77**, 054901 (2008).

[18] J. Brachmann *et al.*, Phys. Rev. C **61**, 024909 (2000).

[19] L. P. Csernai and D. Rohrich, Phys. Lett. B **458**, 454 (1999).

[20] R. Snellings *et al.*, Phys. Rev. Lett. **84**, 2803 (2000).

[21] B. B. Back *et al.* (PHOBOS Collaboration), Phys. Rev. Lett. **97**, 012301 (2006).

[22] B. Abelev *et al.* (CMS Collaboration), Phys. Rev. Lett. **111**, 232302 (2013).

[23] B. I. Abelev *et al.* (STAR Collaboration), Phys. Rev. Lett. **101**, 252301 (2008).

[24] C. Alt *et al.* (NA49 Collaboration), Phys. C **68** 034903 (2003).

[25] H. Liu *et al.* (E877 Collaboration), Phys. Rev. Lett. **84**, 5488 (2000).

[26] L. Adamczyk *et al.* (STAR Collaboration), Phys. Rev. Lett. **112**, 162301 (2014).

[27] K. Aamodt *et al.* (ALICE Collaboration), Phys. Rev. Lett. **105**, 252302 (2010).

[28] S. Sarkar, P. Mali, and A. Mukhopadhyay, Phys. Rev. C **95**, 014908 (2017).

[29] P. F. Kolb, P. Huovinen, U. Heinz, and H. Heiselberg, Phys. Lett. B **500**, 232 (2001).

[30] P. F. Kolb, J. Sollfrank, and U. W. Heinz, Phys. Lett. B **459**, 667 (1999).

[31] S. A. Voloshin and A. M. Poskanzer, Phys. Lett. B **474**, 27 (2000).

[32] H. Caines, Eur. Phys. J. C **49**, 297 (2007).

[33] J. Barrette *et al.* (E877 Collaboration), Phys. Rev. C **51**, 3309 (1995); Phys. Rev. C **55**, 1420 (1997).

[34] A. M. Poskanzer and S. A. Voloshin, Nucl. Phys. A **661**, 341c (1999).

[35] C. Adler *et al.* (STAR Collaboration), Phys. Rev. C **66**, 034904 (2002).

[36] J. D. Bjorken, Phys. Rev. D, **27**, 140 (1983).

[37] H.-J. Drescher *et al.,* Phys. Rev. C **76**, 024905 (2007).

[38] S. Sarkar, P. Mali, and A. Mukhopadhyay, Phys. Rev. C **96**, 024913 (2017).

[39] P. P. Bhaduri and S. Chattopadhyay, Phys. Rev. C **81**, 034906 (2010).

[40] G. Aad *et al.* (ATLAS Collaboration), Phys. Lett. B **707**, 330 (2012).

[41] P. Huovinen *et al.*, Phys. Lett. B **503**, 58 (2001).

[42] U. Heinz, C. Shen, and H. Song, AIP Conf. Proc. **1441**, 766 (2012).

[43] P. Romatschke and U. Romatschke, Phys. Rev. Lett. **99**, 172301 (2007).

[44] M. Luzum and P. Romatschke, Phys. Rev. C **78**, 034915 (2008).

[45] H. Song and U. W. Heinz, Phys. Rev. C **77**, 064901 (2008).